Journal of Physics: Conference Series

PAPER

Numerical Analysis of the Stress State and Fracture of Porous Ceramics at the Mesolevel

To cite this article: V A Mikushina and I Yu Smolin 2019 *J. Phys.: Conf. Ser.* **1214** 012016

View the article online for updates and enhancements.

IOP ebooks™

Bringing you innovative digital publishing with leading voices to create your essential collection of books in STEM research.

Start exploring the collection - download the first chapter of every title for free.

This content was downloaded from IP address 255.255.255.254 on 29/04/2019 at 09:48

IOP Conf. Series: Journal of Physics: Conf. Series **1214** (2019) 012016 doi:10.1088/1742-6596/1214/1/012016

Numerical Analysis of the Stress State and Fracture of Porous Ceramics at the Mesolevel

V A Mikushina[1,2] and I Yu Smolin[1,2]

[1]National Research Tomsk State University, 634050 Tomsk, Russia
[2]Institute of Strength Physics and Materials Science SB RAS, 634055 Tomsk, Russia
E-mail: mikushina_93@mail.ru

Abstract. The paper is devoted to the numerical investigation of inelastic deformation and fracture of porous alumina ceramics. A structural model of the mesovolume is developed with the use of an experimental scanning electron microscopic image. The mechanical behavior of the matrix is described by two constitutive models from plasticity theory and continuum damage mechanics. Uniaxial tension and compression of the mesovolume are numerically simulated in a two-dimensional formulation. The features of fracture patterns in the cases of the two constitutive models adopted are analysed. Effective mechanical characteristics of the studied ceramics are determined from the performed calculations. The results obtained can be used to specify the characteristics of the Drucker–Prager material for macroscopic modeling.

1. Introduction

Currently, porous ceramic products are used in various fields. Compared with porous metals and plastic materials, porous ceramics have several advantages, namely, good resistance to high temperatures and aggressive media, refractory properties, wear resistance as well as low thermal conductivity and low density. Ceramic products have areas of application where their inherent porosity characterized by the size and morphology of pores, their connectivity, permeability, etc. is very important. Pores in the material have both positive and negative effects. For example, on the one hand, they provide the necessary functional properties; on the other hand, they reduce the strength of the material. Therefore, in modeling deformation and fracture of porous materials, account should be taken not only of the porous structure but also of its influence on the mechanical behavior of the material. To do this requires various approaches, one of which is physical mesomechanics of materials [1–7].

Numerical modeling is the most important and actively developed method of investigation of deformation processes in porous media. In contrast to laboratory experiments, numerical modeling is much less resource-consuming and repeatable in different variations.

There exist numerous models to describe the behavior of brittle materials, among which are concrete, rocks, and ceramics. Example models are the Holmquist–Johnson–Cook model [8], Riedel–Hiermaier–Thoma model [9], continuous surface cap model [10], etc. However, the above models were developed and tested in order to describe high strain rates and/or shock loading [11–14]. A classical limit-state criterion for describing fracture or inelastic deformation of brittle and quasi-brittle materials that resist differently under compression and tension is the Drucker–Prager criterion [2, 15]. Not the mere fact of fracture but the process of its development in the material can be effectively described with the concept of continuum damage mechanics where the evolution of damage

Content from this work may be used under the terms of the Creative Commons Attribution 3.0 licence. Any further distribution of this work must maintain attribution to the author(s) and the title of the work, journal citation and DOI.
Published under licence by IOP Publishing Ltd

accumulation is taken into account: local volumes of the material become fractured with damage accumulation. Moreover, these processes are understudied for porous ceramics.

Therefore, the aim of this paper is to numerically investigate the mechanical behavior of porous alumina ceramics at the mesolevel using two models. One is based on the elastic-plastic approach, and the other is on the ideology of damage accumulation. This modeling results in the effective mechanical characteristics of the porous material: shear and bulk moduli, ultimate compressive and tensile stresses. The latter are used to calculate the parameters of the Drucker–Prager plasticity model, which are further helpful in macroscopic modeling to set effective strength properties of the porous material.

2. Model description

Our task is to determine effective elastic and strength characteristics for the macrolevel, i.e. a homogeneous porous material, by modeling the mechanical behavior of a mesovolume with explicit consideration for pores using the homogenization method. Another task is based on the analysis of fracture patterns to determine features of each of the models in relation to the description of mesoscopic fracture and macro–response in the form of averaged loading diagrams under uniaxial compression and tension.

To predict mechanical characteristics of the material, we study mesovolumes with explicit consideration for pores under uniaxial tension and compression. Based on the previous experimental data [16], scanning electron microscopic (hereinafter, SEM) images of porous aluminum oxide ceramics were chosen. Computer geometric models of the mesovolume structure were constructed using SEM images of pores. An example of the SEM image and the obtained structural model are shown in Fig. 1. Here the mesovolume dimensions are 100×100 μm^2; the mesovolume porosity is 17%. The structural model shown in Fig. 1 is the object of investigation in this paper.

For the matrix, we take physical and mechanical characteristics corresponding to nonporous Al_2O_3 (Table 1). Characteristics of the elastic medium are set for the pores, with the elastic moduli three orders of magnitude lower than in the matrix.

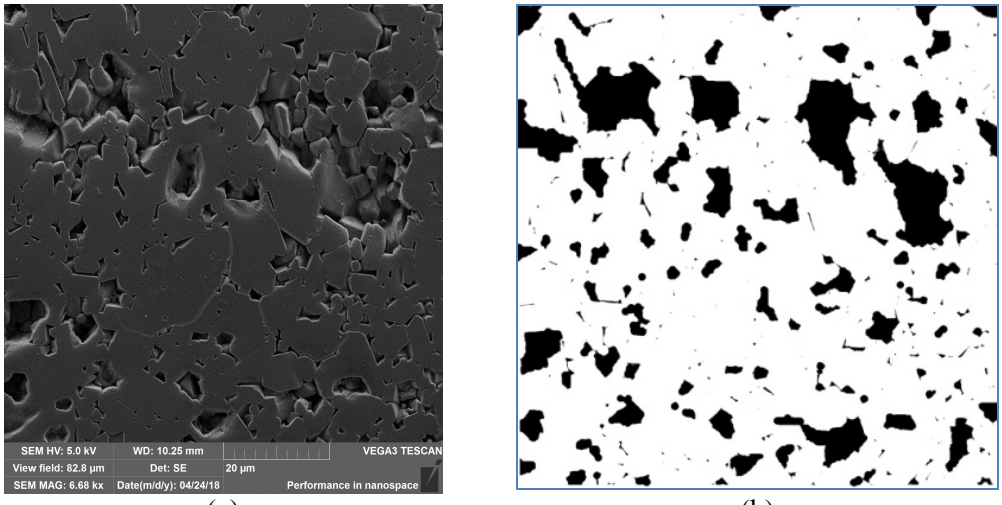

(a) (b)

Figure 1. Scanning electron microscopy of the etched surface of Al_2O_3 specimen (a). A computer model of the ceramic structure with the porosity 17 % (b).

Table 1. Mechanical and physical properties of Al_2O_3-based ceramics.

Density ρ, g/cm^3	Cohesion *Y*, GPa	Bulk modulus *G*, GPa	Shear modulus *K*, GPa	Coefficient of internal friction α
3.98	6.65	251	163	0.4

As the structural models were two-dimensional, the problem of modeling the mechanical behavior was solved in the two-dimensional statement for the plane-strain conditions. Deformation and fracture processes in the studied specimens are computed with the use of the finite-difference method for numerical solution of differential equations of the solid mechanics within the Lagrangian description of a continuum. To perform modeling an original computer code was developed. The mechanical behavior of the material is described by the system of continuum mechanics equations that includes the fundamental conservation laws (1), geometrical relations (2), and constitutive equations

$$\rho V = \rho_0 V_0,\ \rho \dot{v}_i = \sigma_{ij,j} \tag{1}$$

$$2\dot{\varepsilon}_{ij} = v_{i,j} + v_{j,i}\quad 2\dot{\omega}_{ij} = v_{i,j} - v_{j,i} \tag{2}$$

The elastic response is described by the relations of the hypoelastic material model (3)

$$\dot{P} = -K\dot{\theta},\ \dot{s}_{ij} = 2G\left[\dot{\varepsilon}_{ij} - \frac{1}{3}\dot{\theta}\delta_{ij}\right] - s_{ik}\dot{\omega}_{kj} + s_{kj}\dot{\omega}_{ik} \tag{3}$$

Here ρ_0, ρ, V_0, V are the initial and current values of the material density and elementary volume, respectively, v_i are the velocity vector components, σ_{ij} and s_{ij} are the stress and the deviatoric stress tensor components, ε_{ij} are the strain tensor components, P is the pressure, $\theta=\varepsilon_{ii}$ is the bulk strain, G and K are the shear modulus and bulk modulus, respectively, δ_{ij} is the Kronecker symbol, $s_{ik}\dot{\omega}_{kj} + s_{kj}\dot{\omega}_{ik}$ is the rotation correction that occurs when using the corotational Jaumann derivative to the stress tensor.

Inelastic deformation and fracture are modeled using two constitutive models: a model of the elastic-brittle material and a model of the elastic-plastic material. In the elastic-brittle model, we use the governing equations taking account of damage accumulation that is responsible for degradation of elastic properties:

$$G = G_0(1-D)\,,\ K = K_0(1-D) \tag{4}$$

$$D(t) = \int_{t_0}^{t} \frac{\left[H(\mu_\sigma)\left(\sigma - \sigma_0^c\right)^2 + (1-H(\mu_\sigma))\left(\sigma - \sigma_0^t\right)^2\right]dt}{\sigma_*{}^2\left[H(\mu_\sigma)t^c + (1-H(\mu_\sigma))t^t\right]} \tag{5}$$

Here G_0 and K_0 are the initial shear modulus and bulk modulus, respectively, $D(t)$ is the function of the material degradation (damage), $H(\mu_\sigma)$ is the Heaviside function, $\sigma = -\alpha P + \tau$ is the Drucker–Prager stress, α is the coefficient of internal friction, $\tau = (\frac{1}{2}s_{ij}s_{ij})^{1/2}$ is the stress tensor intensity, σ_0^c and σ_0^t are the initial and current stress values at the elastic stage after which the material begins to accumulate damages in the compression and tension regions, respectively, with the constraint $\sigma_0^t << \sigma_0^c$, t^c, t^t are the characteristic fracture time in compression and tension, respectively, and $\sigma_* = \sigma_{0*}(1.01+\mu_\sigma)^2$ is the model parameter defining the damage accumulation rate.

Finally, we take, as the fracture criterion, the condition when the local damage value equals unity.

With the elastic-plastic model, the strain rates in formula (3) present the difference of the total strain rate and plastic strain rate $\theta = \theta_\tau - \theta_p$, $\varepsilon = \varepsilon_\tau - \varepsilon_p$.

The components of the plastic strain rate tensor are determined by the flow rule as

$$\dot{\varepsilon}_{ij}^{p} = \dot{\lambda}\left(\frac{S_{ij}}{2\sqrt{J_2}} + \beta\delta_{ij}\right) \tag{6}$$

with the proviso that $f(\sigma_{ij}) \geq 0$, where

$$f(\sigma_{ij}) = \sqrt{J_2} - \alpha P - Y \tag{7}$$

Here β is the dilatation coefficient, Y is the cohesion, J_2 is the second invariant of the deviatoric stress tensor, and $\dot{\lambda}$ is the nonnegative plastic consistency parameter (multiplier).

In the model of the elastic-plastic material, we take, as the fracture criterion, the ultimate accumulated inelastic strain.

3. Modeling results and discussion

Mesoscopic modeling of deformation and fracture gives effective mechanical characteristics of the porous material, i.e. elastic shear and bulk moduli, ultimate compressive and tensile stresses. The latter data are used to calculate the parameters of the Drucker–Prager plasticity model to set macroscopic properties of the material. As modeling is performed under uniaxial loading in the plane-strain conditions, the formulae for cohesion and the coefficient of internal friction have the form

$$Y = \frac{2\sigma_c\sigma_t\sqrt{1-\nu+\nu^2}}{3(\sigma_c+\sigma_t)}, \alpha = \frac{\sigma_c-\sigma_t}{\sigma_c+\sigma_t}\frac{\sqrt{3(1-\nu+\nu^2)}}{1+\nu} \quad (8)$$

where σ_c and σ_t are the ultimate compressive and tensile stresses, respectively, and ν is the Poisson ratio.

Ultimate compressive and tensile stress values as well as the related parameters of the Drucker–Prager plasticity model are presented in Table 2.

Table 2. Effective mechanical properties of porous alumina ceramics

Constitutive model	σ_t, MPa	σ_c, MPa	Y, MPa	α
Elastic-brittle material	229	704	105	0.66
Elastic-plastic material	266	951	126	0.73

The stress-strain curves in tension and compression are shown in Fig. 2. As one can see, the loading curves averaged over the mesovolume (Fig. 2) have a form characteristic for brittle materials. In the case of the constitutive model of the elastic-brittle material, the strain curves lie below both in compression and tension. The region beyond the ultimate strength is longer in tension as in this case the stress decrease in the fractured cells is more pronounced while in compression the fractured cells continue to resist loading. Graphically, it is shown up in the violation of smoothness of the curves, exhibiting an oscillatory behavior.

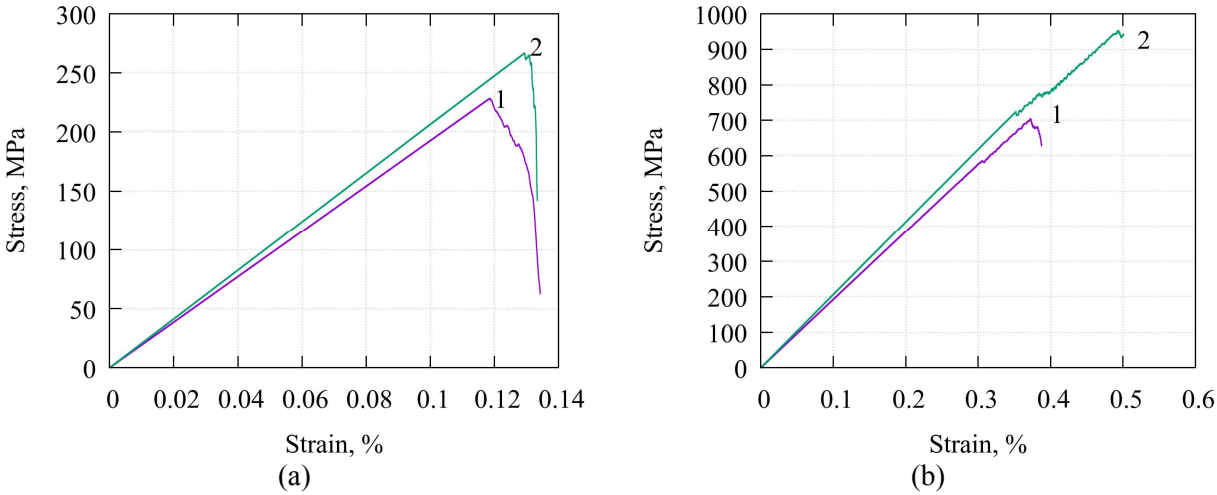

Figure 2. Stress-strain curves in tension (a) and compression (b). Digit 1 corresponds to the elastic-brittle model with damage, and digit 2 is the elastic-plastic model.

The fracture patterns of the investigated mesovolume in compression and tension along the horizontal axis using different models are shown in Figs. 3–4. It can be noted that cracks in the

mesovolume grow in different places depending on the model and type of loading. In compression, fracture patterns are similar for different models: cracks originate in the same places, although propagating in different directions. In tension, fracture occurs in completely different places for the two models. Tensile cracks are perpendicular to the loading direction, and compressive cracks are parallel and at an angle of 45 degrees to the loading direction, which is typical of the behavior of porous brittle materials.

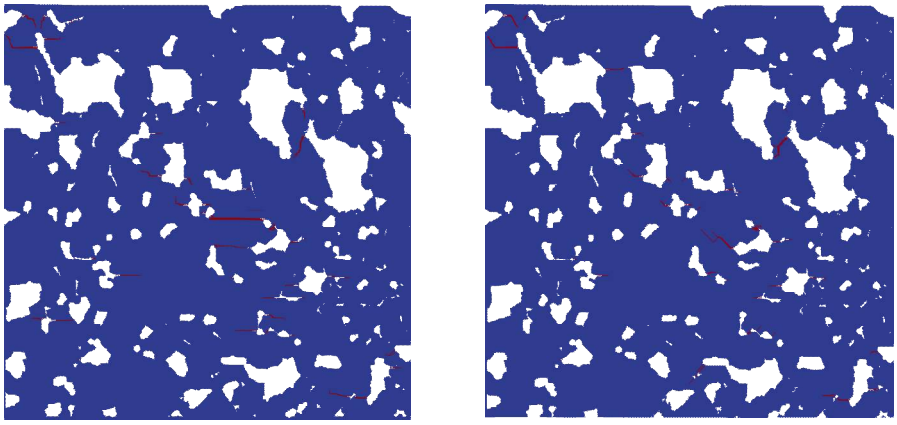

(a) (b)

Figure 3. Fracture patterns in compression: the elastic-brittle model (a) and the elastic-plastic model (b).

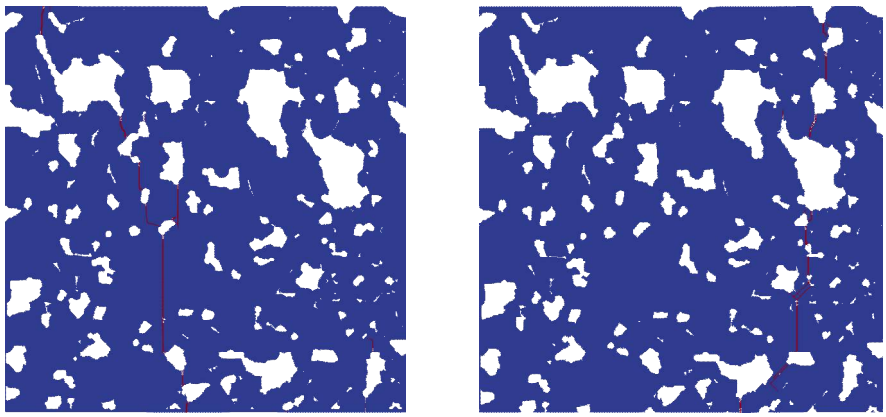

(a) (b)

Figure 4. Fracture patterns in tension: elastic-brittle model (a), elastic-plastic model (b).

The fracture cites in both the models of inelastic deformation and fracture are determined by the features of distribution of the Drucker–Prager stresses. These distributions are shown in Figs. 5–8.

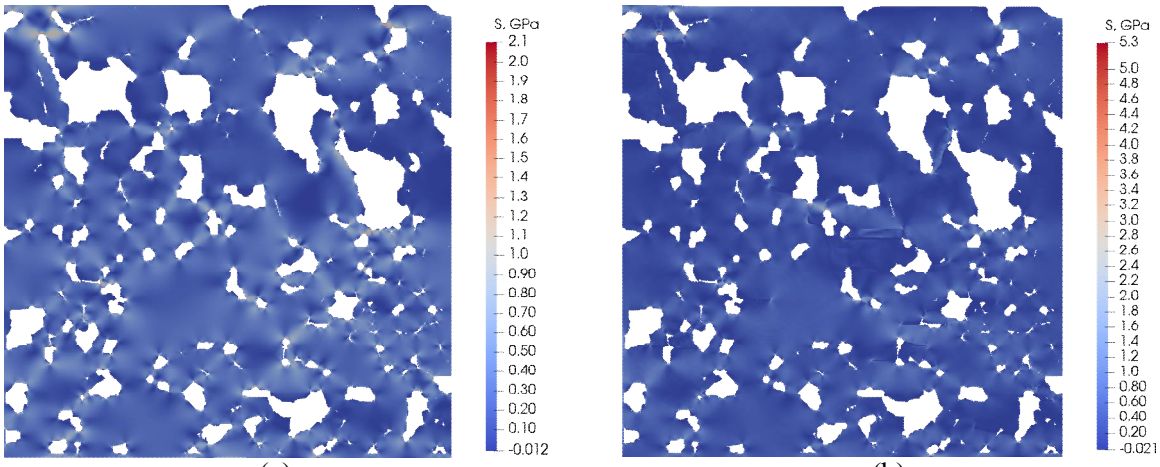

(a) (b)

Figure 5. Distributions of the Drucker–Prager stresses in compression with the use of the elastic-brittle model at the initial (a) and final stages of crack generation (b).

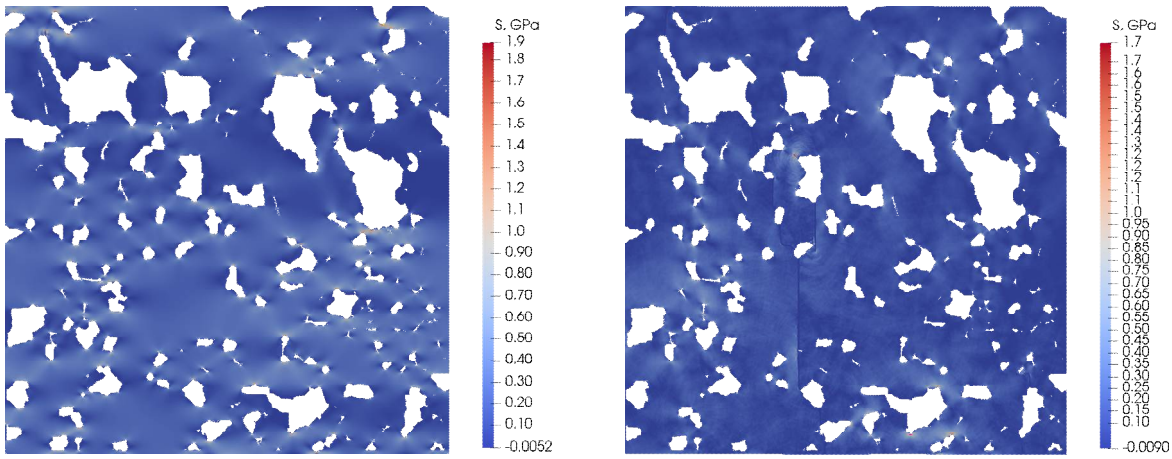

(a) (b)

Figure 6. Distributions of the Drucker–Prager stresses in tension with the elastic-brittle model at the initial (a) and final stages of crack generation (b).

With the elastic-plastic model, the spread of Drucker–Prager stress values is wider due to negative values. Maximum positive values remain the same due to restrictions imposed by the plasticity condition. The most part of the volume is under stresses in the region of average values indicated on the corresponding scale. In contrast, the elastic-brittle model allows for higher stress values (Fig. 7b). However, these areas are very small and few in number, the most part of the volume is under stresses in the region of minimum values. Analyzing Figs. 5–8, one can see that the fracture cites are determined by the maximum Drucker–Prager stresses.

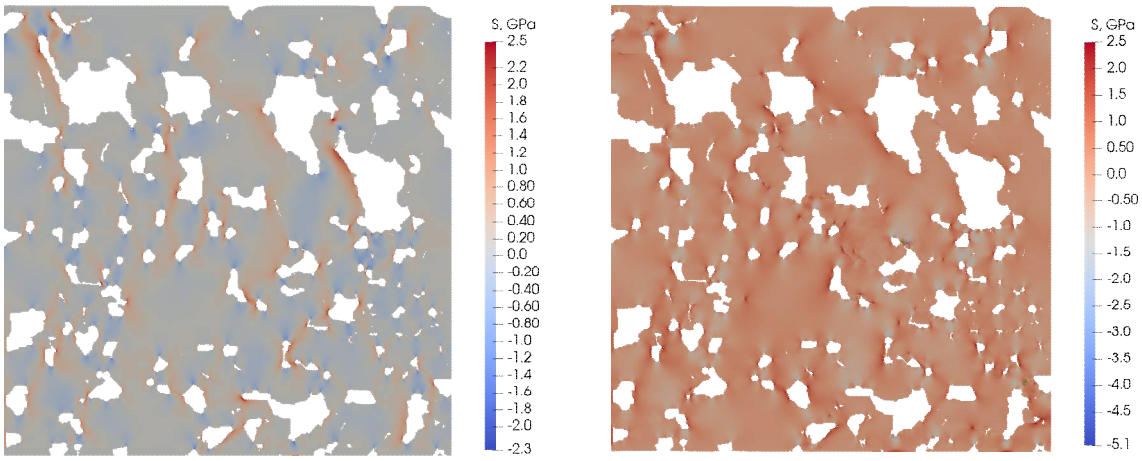

(a) (b)

Figure 7. Distributions of the Drucker–Prager stresses in compression with the elastic-plastic model at the initial (a) and final stages of crack generation (b).

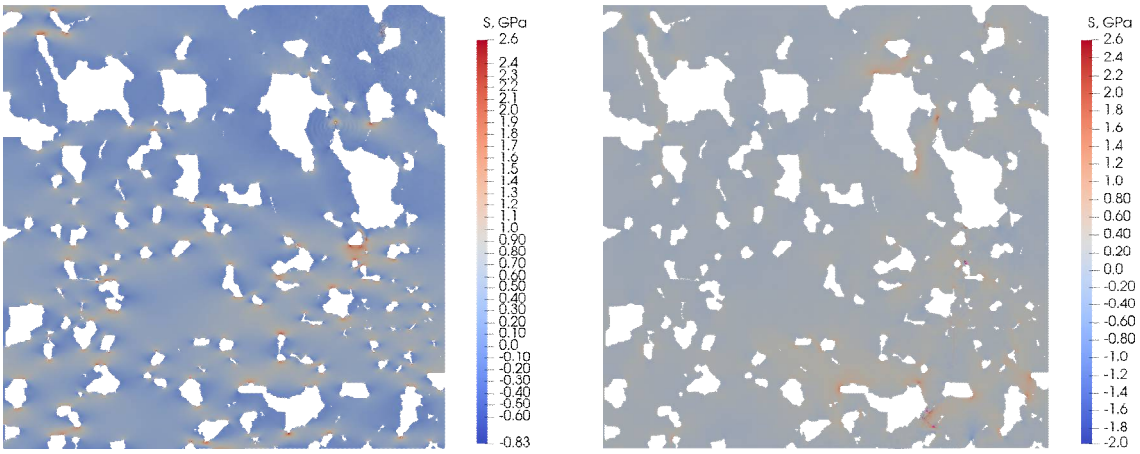

(a) (b)

Figure 8. Distributions of the Drucker–Prager stresses in tension with the elastic-plastic model at the initial (a) and final stages of crack generation (b).

4. Conclusion

The calculations for the two models showed that despite the difference in the distribution of stresses and fracture areas in mesovolumes, the averaged effective characteristics of not only elastic but also strength properties turned out to be close. The paper presents a method for determining the effective characteristics of the Drucker–Prager material model and determines these values for alumina ceramics with a porosity of 17%. In the future, these values can be used in macroscopic modeling by setting the material properties.

Acknowledgments

The work was carried out within the framework of the Fundamental Research Program of the State Academies of Sciences for 2013–2020, line of research III.23, and with the support of the Tomsk State University Competitiveness Improvement Program.

References

[1] Konovalenko Ig S, Smolin A Yu, Korostelev S Yu and Psakh'e S G 2009 *Tech. Phys.* **54** (5) 758–761

[2] Kostandov Yu A, Makarov P V, Eremin M O, Smolin I Yu and Shipovskii I E 2013 *Int. Appl. Mech.* **49**(1) 95–101
[3] Dmitriev A I, Smolin A Yu, Popov V L and Psakhie S G 2009 *Phys. Mesomech.* **12**(1-2) 11–19
[4] Karakulov V V, Smolin I Yu and Skripnyak V A 2014 *AIP Conf. Proc.* **1623** 237–240
[5] Cherepanov O I, Smolin I Yu, Stefanov Yu P and Makarov P V 1999 *Comput. Mater. Sci.* **16** 25–31
[6] Somnath G, Lee K and Raghavan P 2001 *Int. J. Solids Struct.* **38**(14) 2335–2385
[7] Mikushina V A, Sidorenko Y N 2015 *AIP Conf. Proc.* **1683** 020150
[9] Holmquist T J, Johnson G R and Cook W H 1993 *Proc. 14th Int. Symposium on Ballistic* vol 2 (Arlington: ADPA) pp 591–600
[9] Riedel W, Kawai N and Kondo K 2009 *Int. J. of Impact Eng.* **36**(2) 283–293
[10] Murray Y D, Abu-Odeh A and Bligh R 2007 *Users manual for LS-DYNA concrete material model 159* report FHWA-HRT-05-062 (McLean: Federal Highway Administration) p 89
[11] Orlov M Y, Glazyrin V P and Orlov Yu N 2017 *AIP Conf. Proc.* **1893** 030133
[12] Glazyrin V P, Orlov M Yu and Orlov Yu N 2006 *AIP Conf. Proc.***849** 421–426
[13] Skripnyak E G, Skripnyak V A and Skripnyak V V 2012 *AIP Conf. Proc.* **1426** 1157–1160
[14] Skripnyak V A; Skripnyak E G; Kozulin A A, Skripnyak V V and Korobenkov M V 2009 *Russ. Phys. J.* **52**(12) 1300–1308
[15] Makarov P V, Eremin M O 2013 *Frattura ed Integrita Strutturale* **24** 127–137
[16] Kulkov A S, Smolin I Yu and Mikushina V A 2018 *AIP Conf. Proc.* **2051** 020162